Real-Time Optical Spectrum Analysis Based on the Time–Space Duality in Chirped Fiber Gratings

José Azaña, *Student Member, IEEE,* and Miguel A. Muriel, *Senior Member, IEEE*

Abstract—Based on time–space duality, we deduce a time-domain equivalent to the Fraunhofer (far-field) approximation in the problem of spatial diffraction. We can use this equivalence to carry out a real-time optical spectrum analysis, which is shown to be realizable by using, as the dispersive media, filtering devices based on chirped distributed resonant coupling. In particular, we present the design of linearly chirped fiber gratings (reflection configurations) and linearly chirped intermodal couplers (transmission configurations) to work as real-time spectrum analyzers. The proposed systems are shown to work properly by means of simulation tools. Furthermore, we use joint time–frequency signal representations to get a better understanding of the physical processes that determine the behavior of these systems. In this way, we demonstrate that the propagation of a given signal through a chirped fiber grating (or a chirped intermodal coupler), under the temporal Fraunhofer conditions, translates into a temporal separation of the spectral components of the signal. The results of our study indicate potential important applications based on this effect.

Index Terms—Fourier transforms, gratings, optical fibers, optical fiber devices, time-domain analysis, transient propagation.

I. INTRODUCTION

DEVELOPMENT of short-pulse laser technology continuously increases the areas of application of temporal optics in signal processing, optical communications, and other scientific areas. One of the main tasks in these applications consists of the ability to control, modify, and analyze the form of optical pulses. For this purpose, it is especially useful to find temporal analogs of the signal processing tools which have already been used in spatial optics.

There exists a well-known analogy between the equations that describe the paraxial diffraction of beams in space and the temporal dispersion of narrow-band pulses in a dielectric [1]–[3]. Several authors have used this similarity to propose and create temporal analogs of spatial systems [4]–[15]. T. Jannson and J. Jannson [4] demonstrated that a temporal self-imaging effect (the Talbot effect) might exist in single-mode fibers and they proposed using this effect for transference of the information contained in periodic signals. Saleh and Irshid [5] applied a time-domain Collett–Wolf equivalence theorem to pulse propagation in fibers. The time–space duality has led to the conclusion that an element that provides quadratic phase modulation

in time is the analog of a thin lens in space. These elements are known as time lenses. In that sense, T. Jannson [6] theoretically proposed the implementation of real-time Fourier transformation based on a temporal equivalence with the spatial Fourier transformation that uses spatial lens. For this purpose, he used single-mode optical fibers as the dispersive elements (equivalents to free space) and chirping lasers to provide the required quadratic phase modulation (time lens). Kolner and Nazarathy [7], [8] proposed a temporal imaging system based on a time lens bounded by dispersive media, which allows for distortionless magnification or compression of optical power waveforms. Their system uses an electrooptic phase modulator as the time lens. Furthermore, they derived equivalent expressions for the focal length and the f-number of a time lens. Practical implementations of similar imaging systems have been demonstrated in [9] and [10]. Recently, it has been shown that the time–space duality also applies to the reflection of pulses from linearly chirped fiber gratings (LCFG's), and several applications have been proposed based on this idea [12]–[15].

Here, we present a detailed study of the time-domain formulation equivalent to spatial Fraunhofer diffraction and its application to design real-time optical Fourier transformer systems [12], [13]. The proposed systems do not require quadratic phase modulation. The only requirement is an appropriate filtering configuration working as the dispersive media. To first order, the temporal Fourier transformation can be carried out by use of any filtering scheme that closely provides flat amplitude and linear group delay over the bandwidth of the pulses to be processed. Such a filter can be obtained using single-mode optical fiber [4]–[6], and any of the proposed configurations for dispersion compensation in optical fiber links and for pulse compression [16]–[21]. However, the implementation of the temporal Fraunhofer approximation also requires components that provide both high dispersion and bandwidth large enough to cover the pulse bandwidth. The design of an optical fiber which verifies the required dispersion conditions leads, in general, to too long a distance for a practical implementation, whereas the requirements of dispersion and bandwidth are usually contradictory in a resonant system (the higher the dispersion, the narrower the bandwidth). These drawbacks have been overcome with filtering configurations that use chirped distributed resonant coupling [18], such as LCFG [19] and the linearly chirped intermodal coupler (LCIC) [20]. In the design of these components, the two requirements (dispersion and bandwidth) can be fixed independently, making them optimal candidates for the practical implementation of the time-domain Fraunhofer conditions. In this paper, we demonstrate that the propagation of a given signal through a LCFG or a LCIC, whose dispersion

characteristics are specifically designed to verify the temporal Fraunhofer conditions, translates into a temporal separation of the spectral components of the signal. This effect is, in fact, responsible for the real-time power spectrum analysis provided by these devices. In particular, we carry out a detailed analysis of the effect by using joint time–frequency signal representations [22], [23]. The results of our theoretical study indicate a potential of important applications based on the described effect, such as real-time spectral filtering, temporal pulse shaping, and new techniques for dispersion measurements.

The paper is structured as follows. Section II is devoted to a detailed study of the time–space duality. We use this duality in our deduction of the temporal formulation equivalent to the spatial Fraunhofer diffraction. Section III analyzes the design method of real-time Fourier transformers based on the time-domain Fraunhofer approximation. We present the design method for LCFG's (reflection configuration) as well as for LCIC's (transmission configuration), by using a unified approach. In Section IV, we present an example of the design of a real-time Fourier transformer system. We analyze the performance of this system for different input signals, by using well-proved simulation tools. We include a joint time–frequency analysis of the input and output signals to get a better understanding of the physical processes which determine the behavior of the considered systems. From the results, we also discuss several potential applications of real-time spectrum analysis. Finally, in Section V, we point up some conclusions.

II. THEORY

In this section, we use the well-known time–space duality to present a temporal formulation equivalent to Fraunhofer diffraction. This formulation enables us to carry out a real-time power spectrum analysis.

Firstly, let us review the analogy between the free-space Fresnel diffraction and the distortion of a temporal signal in the first-order dispersion approximation [1]–[3]. On the one hand, the propagation of monochromatic light of wavelength λ over a distance d, under Fresnel conditions (paraxial diffraction), is described by a linear system with an amplitude impulse response $h_d(x, y)$ according to the expression [24]

$$h_d(x, y) = h_{\text{space}} \exp\left(-j\,\frac{\pi}{\lambda d}\,\left(x^2 + y^2\right)\right) \tag{1}$$

where $h_{\text{space}} = (j/\lambda d) \exp(-j(2\pi/\lambda)\,d)$, and x and y represent the Cartesian coordinates in planes transverse to the propagation direction z.

On the other hand, dispersive media in the linear regime can be characterized by means of a transfer function $H(\omega) = |H(\omega)| \exp(-j\Phi(\omega))$. We center our attention on the distortion of a pulsed plane wave centered at the angular frequency ω_0. The analytical signal representation of this pulse is $a_1(t) = \widehat{a}_1(t) \cdot \exp(j\omega_0 t)$, where $\widehat{a}_1(t)$ represents the complex envelope of the signal. Let the transfer function $H(\omega)$ have constant amplitude $|H(\omega)| = H_0$ and quadratic phase response (linear group delay) over the spectral bandwidth of the pulse $a_1(t)$. In this case, the transfer function for the complex

envelopes $\widehat{H}(\omega') = H(\omega_0 + \omega')$, over the pulse's bandwidth, takes the form

$$\widehat{H}(\omega') = H(\omega_0 + \omega') = H_0 \exp(-j\Phi_0) \exp(-j\dot{\Phi}_0\omega')$$
$$\cdot \exp\left(-j\,\frac{1}{2}\,\ddot{\Phi}_0\omega'^2\right) \tag{2}$$

where $\Phi_0 = \Phi(\omega_0)$, $\dot{\Phi}_0 = \partial\Phi/\partial\omega$ for $\omega = \omega_0$, and $\ddot{\Phi}_0 = \partial^2\Phi/\partial\omega^2$ for $\omega = \omega_0$. Notice that we have used the Taylor expansion of the phase function $\Phi(\omega)$ in the vicinity of ω_0. The related impulse response $\widehat{h}(t)$ can then be obtained by taking the inverse Fourier transform of this transfer function

$$\widehat{h}(t_R) = h_{\text{time}} \exp\left(j\,\frac{1}{2\ddot{\Phi}_0}\,t_R^2\right) \tag{3}$$

where $t_R = t - \dot{\Phi}_0$ and $h_{\text{time}} = H_0 \exp(-j\Phi_0)(1/\sqrt{j2\pi\ddot{\Phi}_0})$. The constant $\dot{\Phi}_0$ (group delay) denotes the average pulse delay. The constant $\ddot{\Phi}_0$ (first-order dispersion coefficient), slope of the linear group delay characteristic, is responsible for the pulse shape distortion. The complex envelope $\widehat{a}_2(t)$ of the output pulse may be obtained by convolving the complex envelope $\widehat{a}_1(t)$ of the input pulse with the impulse response function $\widehat{h}(t)$. The temporal impulse response in (3) has the same mathematical structure as the spatial impulse response in (1), which shows that the distortion of a pulse in dispersive media because of first-order chromatic dispersion is mathematically identical to Fresnel diffraction.

According to our initial considerations, (3) describes pulse distortion in dispersive media that closely provide constant amplitude response and quadratic phase response (linear group delay) over the pulse's bandwidth. For example, the equation describes the narrow-band pulse propagation through a single-mode optical fiber. As a result, (3) is also valid for describing the pulse distortion in the different filtering configurations that have been proposed for chromatic dispersion compensation in optical fiber. In this context, we work with optical filters based on chirped distributed resonant coupling [18]: the LCFG [19] and the LCIC [20]. An LCFG (or LCIC) provides the required optical properties (i.e., flat amplitude and linear group delay) within the grating's reflected (transmitted, for the LCIC case) bandwidth. As a result, (3) (the fundamental relation of the time–space duality) describes the interaction between the LCFG (LCIC) and an incident pulse when the pulse's bandwidth is narrower than that of the grating. Furthermore, these filters (LCFG or LCIC) can be specifically designed to get exactly the required amount of dispersion over the desired bandwidth, which makes these devices optimal components to use in the design of time-domain analogs of spatial systems [12]–[15]. In particular, we study the design of the aforementioned devices to work as power spectrum analyzers [12] by using a time formulation equivalent to the spatial Fraunhofer approximation.

For free-space propagation, it is well known that if the propagation distance d is sufficiently long, the field complex amplitude in the plane $z = d$ is, within a phase factor, proportional to the two-dimensional (2-D) Fourier transform of the field complex amplitude in the input plane $z = 0$ [24]. This approxima-

tion is valid if the input field is confined to a circle of radius Δx_1, which satisfies the condition

$$\frac{\Delta x_1^2}{\lambda d} \ll 1 \qquad (4)$$

which is known as the Fraunhofer (far-field) approximation.

Now we turn our attention to the temporal pulse distortion in dispersive media (LCFG or LCIC). Let us assume that the input pulse's bandwidth is narrower than the grating's bandwidth. As we have seen in this case, the complex envelope $\widehat{a}_2(t)$ of the output pulse can be obtained by convolving the complex envelope $\widehat{a}_1(t)$ of the input pulse with the impulse response function $\widehat{h}(t)$ in (3). We obtain

$$\widehat{a}_2(t_R) = h_{\text{time}} \int_{-\infty}^{+\infty} \widehat{a}_1(t') \exp\left(j\frac{1}{2\ddot{\Phi}_0}(t_R - t')^2\right) dt'$$

$$= h_{\text{time}} \exp\left(j\frac{1}{2\ddot{\Phi}_0}t_R^2\right) \int_{-\infty}^{+\infty} \widehat{a}_1(t')$$

$$\cdot \exp\left(j\frac{1}{2\ddot{\Phi}_0}t'^2\right) \exp\left(-j\frac{1}{\ddot{\Phi}_0}t_R t'\right) dt'. \qquad (5)$$

If $\widehat{a}_1(t)$ is confined to a small time width Δt_1, and if the dispersion coefficient $\ddot{\Phi}_0$ is sufficiently large so that

$$\left|\frac{\Delta t_1^2}{2\pi\ddot{\Phi}_0}\right| \ll 1 \qquad (6)$$

then the phase factor $(t'^2/2\ddot{\Phi}_0) \leq (\Delta t_1^2/2\ddot{\Phi}_0)$ is negligible and (5) may be approximated by

$$\widehat{a}_2(t_R) = h_{\text{time}} \exp\left(j\frac{1}{2\ddot{\Phi}_0}t_R^2\right) \int_{-\infty}^{+\infty} \widehat{a}_1(t')$$

$$\cdot \exp\left(-j\frac{1}{\ddot{\Phi}_0}t_R t'\right) dt'$$

$$= h_{\text{time}} \exp\left(j\frac{1}{2\ddot{\Phi}_0}t_R^2\right) [\widehat{A}_1(\omega)]_{\omega = t_R/\ddot{\Phi}_0} \qquad (7a)$$

$$\widehat{A}_1(\omega) = F(\widehat{a}_1(t)) \qquad (7b)$$

where F denotes the Fourier transform. Hence, under the conditions of inequality (6), the output pulse envelope is, within a phase factor, proportional to the Fourier transform of the input pulse envelope, evaluated at the angular frequency

$$\omega = \frac{t_R}{\ddot{\Phi}_0}. \qquad (8)$$

Inequality (6) is the time-domain analog of the spatial Fraunhofer condition (4) and is valid if the first-order dispersion coefficient of the grating, $\ddot{\Phi}_0$, is much greater than the square of the input pulsewidth Δt_1. It is worth noting that only the magnitude of the Fourier transform is recovered, since the phase of the output signal is complicated by the additional term $\exp(j(1/2\ddot{\Phi}_0)t_R^2)$.

In conclusion, if the temporal Fraunhofer condition [inequality (6)] is verified, we can assert that the average optical power of the output pulse $P_2(t_R) = |\widehat{a}_2(t_R)|^2$ is proportional to the energy density spectrum (squared magnitude of the signal

Fourier transform) of the input complex envelope $\widehat{a}_1(t)$ evaluated at $\omega = t_R/\ddot{\Phi}_0$. The effect can be explained as follows. The reflection of an incident signal upon the LCFG (LCIC) does not essentially affect the power spectrum of this signal; however, the different spectral components of the signal undergo a temporal realignment process according to the group delay characteristic of the grating (i.e., dispersion causes different frequencies to travel at different velocities). The time-domain Fraunhofer condition ensures that this dispersive effect is strong enough to temporally separate the spectral components of the original signal. In this way, although the phase of the signal spectrum is not directly obtained from the propagation through the dispersive element, the resultant signal contains the total input spectral information (including magnitude and phase) along the time axis. For instance, a spectral filtering of the original signal can be carried out, from the resultant signal after the propagation, by using time-division techniques: by taking the appropriate time interval and compensating the dispersion introduced by the grating (using the complementary grating), we can filter the original signal through the desired passband. In our numerical investigation (Section IV), we analyze with more detail the described effect by using a joint time–frequency representation of the signals involved in the processes.

III. DESIGN OF POWER SPECTRUM ANALYZERS

In this section, we analyze the implementation of the Fourier transformation based on a temporal formulation equivalent to the spatial Fraunhofer diffraction by using all-fiber filters based on chirped distributed resonant coupling (LCFG and LCIC) [18]–[20].

The LCFG and the LCIC provide a propagation delay that is a linear function of frequency, which is achieved by coupling energy between two modes with different group velocities in such a way that the coupling location varies linearly in frequency. These devices consist of a periodic perturbation of the refractive index along the fiber length, which is formed by exposure of the core to an intense optical interference pattern. The required distributed coupling location is achieved if the period of the perturbation is linearly chirped. The difference between the two components is that the LCFG is based on counterdirectional coupling in single-mode fiber whereas the LCIC uses co-directional coupling between two modes (LP$_{01}$ and LP$_{02}$, in practice) in a few-mode fiber. Therefore, the LCFG works as a reflective device whereas the LCIC works in transmission. At this point, it is worth noting that similar filters can be fabricated within a waveguide.

For the design of this type of filter, it is convenient to define the parameter τ or time delay between the two coupled modes over a unit length, i.e., $\tau = |1/v_{g1} - 1/v_{g2}|$, where v_{g1} and v_{g2} are the group velocities of the two modes. For the calculation of the parameter τ, the waveguide and material dispersions of the fiber are not usually considered, i.e., the group velocities v_{g1} and v_{g2} are assumed to be constant with frequency. Under these conditions, in the LCFG $v_{g1} = -v_{g2} = c/n_m$ and therefore $\tau = 2n_m/c$, c being the speed of light in vacuum and n_m being the effective refractive index of the single mode. In the LCIC, the parameter τ depends on the normalized frequency or
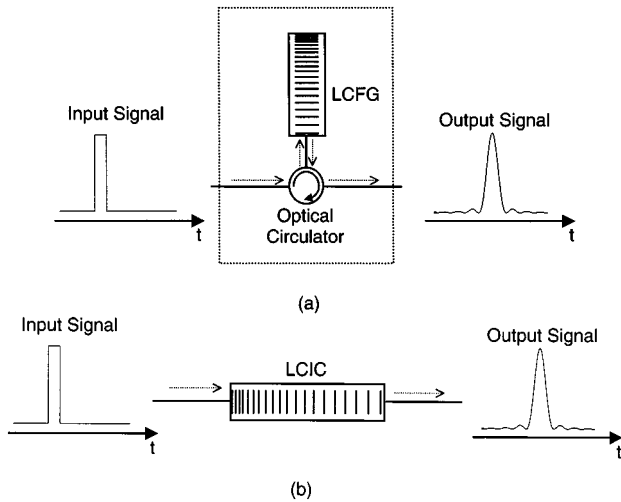
Fig. 1. Diagram of the proposed configurations for the implementation of real-time optical spectrum analysis. (a) Reflection configuration based on LCFG. (b) Transmission configuration based on LCIC.

fiber parameter V [20]. Let $\Omega(z)$ be the local spatial angular frequency of the grating (z being the fiber distance). In the case of a linearly chirped period, $\Omega(z)$ can be expressed as

$$\Omega(z) = Cz + \Omega_0, \qquad \frac{-L}{2} \le z \le \frac{L}{2} \qquad (9)$$

where C denotes the chirp factor of the grating and L is the length of the coupling region. Ω_0 fixes the center frequency ω_0 of the grating spectral band, since, according to the Bragg condition, $\Omega_0 = \omega_0 \tau$. The chirp factor C determines the dispersion coefficient of the filter $\ddot{\Phi}_0$ according to the expression $C = \pm \tau^2 / \ddot{\Phi}_0$, where the positive sign corresponds to the LCFG and the negative one corresponds to the LCIC. The critical design parameter is the device length L since it depends on both requirements, the magnitude of the dispersion coefficient $|\ddot{\Phi}_0|$ and grating bandwidth $\Delta\omega$, according to the expression $L = |\ddot{\Phi}_0|\Delta\omega/\tau$. The reader can find a detailed description of the stated relations between the dispersion characteristics of the grating and the perturbation parameters in [18]. To obtain such relations, it is assumed that the waves are coupled exactly at the point where the phase-matching condition is verified for each frequency.

Next we present the design of the LCFG and the LCIC to provide a real-time optical spectrum analysis. Fig. 1 shows a diagram of the proposed configurations for the implementation of the Fourier transformation, using a LCFG [Fig. 1(a)] and LCIC [Fig. 1(b)]. The main disadvantage of the LCFG is that it is a reflective device, requiring an optical circulator to retrieve most of the reflected signal. Input Signal in the figure labels the average optical power of the pulse entering in the corresponding device, $P_1(t) = |\hat{a}_1(t)|^2$. Output Signal in the figure labels the average optical power of the output pulse, $P_2(t) = |\hat{a}_2(t)|^2$.

In the case of single pulses, the devices must be designed to verify the time-domain Fraunhofer approximation for a given pulse time-width. Let Δt_1 be the time-width of the input pulses to be processed. We must design a filter that provides a linear group delay whose slope (dispersion coefficient) satisfies

$|\ddot{\Phi}_0| \gg \Delta t_1^2/2\pi$ [time-domain Fraunhofer approximation in inequality (6)] over a spectral bandwidth broader than the pulse's bandwidth ($\Delta\omega > 2\pi/\Delta t_1$). At this point, it is important to note that, even if the designed grating bandwidth is narrower than the pulse bandwidth, the Fourier transformation is carried out although this analysis only extends over the designed bandwidth $\Delta\omega$. The grating filters (LCFG or LCIC implementations) will provide the required dispersion characteristic if its chirp factor C and length L satisfy the following conditions:

$$|C| \ll \frac{2\pi\tau^2}{\Delta t_1^2} \qquad (10)$$

and

$$L \gg \frac{\Delta t_1}{\tau}. \qquad (11)$$

The required device length only depends on the pulse timewidth: the larger the pulsewidth, the longer the required device. In practice, the parameter τ in the LCFG is larger than the parameter τ in the LCIC, which means that the resultant LCIC structure is longer than the corresponding LCFG. This is the main disadvantage of the LCIC: the fabrication of sufficiently long LCIC structures may constitute a serious problem, since it is very difficult to maintain the required uniformity of the design parameters over long lengths [18].

In the case of pulse sequences, the magnitude of the grating dispersion coefficient $|\ddot{\Phi}_0|$ has to be sufficiently large to ensure that the temporal Fraunhofer condition is verified for the total duration of the sequence. Furthermore, the grating bandwidth must be broader than the largest bandwidth of the individual pulses that constitute the sequence.

IV. NUMERICAL RESULTS AND DISCUSSIONS

In this section, we present an example of implementation of time-domain Fraunhofer approximation. In particular, we design an LCFG (reflection configuration) to work as a Fourier-transformer system for pulses with time widths $\Delta t_1 = 1$–10 ps. This design works properly also for pulse sequences if the total duration of the sequence is not longer than 10 ps. We have tested this design with different input signals by use of simulation tools. Furthermore, we use joint time–frequency representations of the signals to get a better understanding of the physical effects that determine the performance of the proposed system and its potential applications. Taking into account that the maximum time width of the pulses to be processed is 10 ps, the LCFG must provide a dispersion which, under the Fraunhofer approximation conditions, satisfies $|\ddot{\Phi}_0| \gg (1/2\pi) \times 100$ ps^2/rad [inequality (6)]. The minimum time width of the pulses (1 ps) determines the grating bandwidth, i.e., $\Delta\omega > 2\pi \times 10^{12}$ rad/s. In particular, the LCFG is designed to provide a positive dispersion coefficient $\ddot{\Phi}_0 = (1/2\pi) \times 10^3$ ps^2/rad over a 1200-GHz bandwidth centered at frequency 193.1 THz ($\lambda = 1552.524$ nm). Taking $n_m = 1.4522$ as the effective refractive index of the grating (1.452 being the core refractive index without perturbation, and 4×10^{-4} being the maximum index modulation of the perturbation), we obtain a time
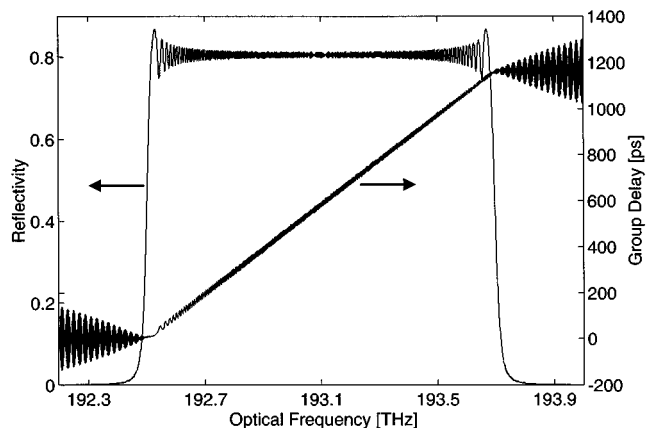
Fig. 2. Reflection spectral characteristics of the LCFG designed to process pulses with time widths from 1 to 10 ps. Left axis: LCFG reflectivity versus optical frequency. The grating has a 1.2-THz bandwidth centered at 193.1 THz. Right Axis: LCFG reflection group delay. The grating provides a linear group delay with a slope (dispersion coefficient) of 10^3 ps^2.

delay over a unit length equal to $\tau = 2n_m/c \approx 9.69$ ns/m. Therefore, the LCFG with the required characteristics has a chirp factor $C = \tau^2/\ddot{\Phi}_0 \approx 600 \times 10^3$ rad/m^2 and length $L = \ddot{\Phi}_0 \Delta\omega/\tau \approx 12$ cm. The grating spatial frequency is centered at $\Omega_0 = \omega_0\tau \approx 11.76$ rd/μm. As result, the grating period varies from 536.21 nm to 532.89 nm. It is worth noting that an LCIC (transmission configuration) providing similar dispersion characteristics requires a length of the order of 6 m, which could be too long for a practical implementation.

We compute the LCFG field reflection coefficient $H(\omega) = |H(\omega)| \exp(-j\Phi(\omega))$ by use of the model proposed in [25], which is based on the transfer matrix formalism and thin-film-filter computational techniques. Fig. 2 shows the LCFG reflectivity $R(\omega) = |H(\omega)|^2$ (left axis) and group delay $t_g(\omega) = \partial\Phi(\omega)/\partial\omega$ (right axis). It can be observed that the grating provides the required features. Notice, however, that the amplitude and group delay responses exhibit undesirable high-frequency ripples around their respective mean value. These ripples can be reduced (or even eliminated) by an appropriate apodization of the grating's refractive index perturbation [26], although in this case the ripples do not affect practically the expected results. It has been demonstrated that the effect of the ripples becomes less noticeable for broader grating bandwidths [26], which is the case for our application. Thus, in most of the cases, the apodization process is not required to avoid the influence of such ripples. Nevertheless, the fabrication process of the gratings introduces stochastic fluctuations on the group delay and reflectivity responses, which, in principle, cannot be completely eliminated [27]. Particularly important are the time delay fluctuations (roughly 15–20 ps). However, when the gratings are used as real-time Fourier transformers, these fluctuations could be ignored under the conditions described below. The time delay Δt_g between the faster frequency of the incident pulse and the slower one can be estimated as $\Delta t_g \approx |\ddot{\Phi}_0|\Delta\omega_{\text{pulse}}$, where $\Delta\omega_{\text{pulse}}$ represents the bandwidth of the pulse. Obviously, for the estimation of the time delay Δt_g, we have to use the grating's bandwidth $\Delta\omega$ instead of the pulse's bandwidth $\Delta\omega_{\text{pulse}}$ when $\Delta\omega_{\text{pulse}} > \Delta\omega$. The ripples around the mean group delay characteristic do not affect essentially the operation of the grating as
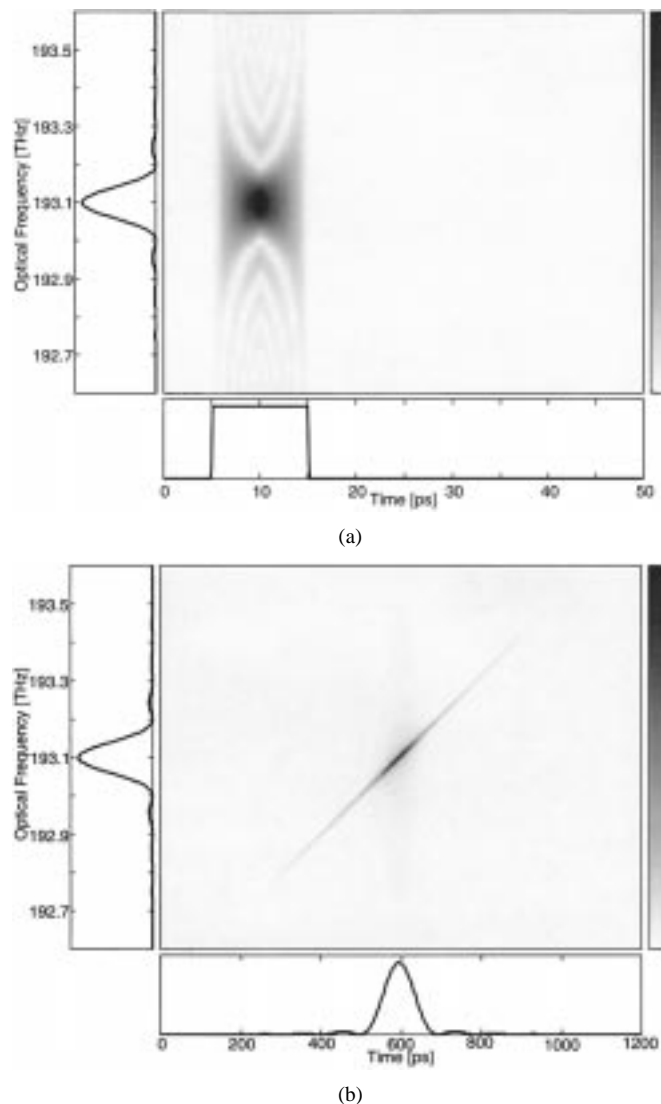

(a)

(b)

Fig. 3. Results from the simulation of the real-time spectrum analyzer, taking, as the input signal, an ideal 10-ps-wide squared pulse. (a) Input signal: the plot at the bottom shows the signal in the time domain. The plot on the left shows the signal in the frequency domain. The larger plot shows the joint time–frequency representation of the signal by using the Wigner–Ville distribution. (b) Output signal, with the same definitions as for (a).

Fourier transformer if their maximum amplitude (peak to peak) can be neglected as compared with the estimated time delay Δt_g, i.e., if this amplitude is less than 10% of Δt_g. It is worth noting that the experimental demonstration of real-time Fourier transformation using an unapodized LCFG has confirmed the stated criterion [13].

We now test the design by simulating the system response to different input signals. In the simulations, we assume that the signals are centered at the central frequency of the grating bandwidth, 193.1 THz. We first obtain the output (reflected) signal spectrum by multiplying the grating frequency response $H(\omega)$ with the input signal spectrum. The corresponding time waveforms can then be recovered by taking the inverse Fourier transforms.

The first example deals with the LCFG response to a 10-ps-wide ideal squared pulse. Fig. 3(a) shows the input signal in both time and frequency representations as well as in the two

domains simultaneously (joint time–frequency representation). The plot at the bottom of the figure represents the average optical power, $P_1(t) = |\widehat{a}_1(t)|^2$, of the input signal in normalized units. The plot at the left of the figure shows the normalized energy density spectrum, $|\widehat{A}_1(\omega)|^2$, of this signal. To obtain a deep insight into the signal structure, this is also represented in both time and frequency domains simultaneously. The larger plot in the upper right of the same figure shows the joint time–frequency energy distribution of the signal. The 2-D distribution intensity is represented by the relative brightness levels of the plot. Such a representation provides temporal location information of the signal's spectral components. For this first case, we have used the Wigner–Ville distribution [22], [23]. Fig. 3(b) shows the signal at the system's output using a similar representation. The plot at the bottom of the figure represents the normalized average optical power $P_2(t) = |\widehat{a}_2(t)|^2$ of the output signal. As expected, the time waveform of this signal is proportional to the spectrum (sinc function) of the input signal. The resultant output power $P_2(t)$ coincides with the input energy density spectrum $|\widehat{A}_1(\omega)|^2$ [by using the scale change defined in (8)]. The plot at the left of the figure represents the normalized energy density spectrum $|\widehat{A}_2(\omega)|^2$ of the signal. Notice that the spectrum amplitude only undergoes a weak distortion compared to the input signal, which is due to the ripple of the grating reflectivity characteristic. Again, the larger plot shows the Wigner–Ville distribution of the considered signal. It is observed that the output (reflected) signal retains spectral components identical to those of the incident signal (except for the mentioned distortion); these components, however, undergo a temporal realignment process according to the group delay characteristic of the dispersive element (LCFG). The temporal Fraunhofer condition ensures that this temporal realignment is sufficiently strong so that only a single dominant frequency term exists at a given instant of time. The effect is observed in the TF diagram: each signal distributes its energy along a straight line (following the group-delay curve). This effect explains the resultant real-time power spectrum analysis and provides additional abilities to control and modify the form of temporal optical pulses. For instance, as described above, the observed effect can be applied to carry out a spectral filtering of the original signal by using time-division techniques on the resultant signal after the propagation.

In order to provide a complete analysis of the described processes, we study the case of an input pulse with a time-width broader than that required for Fourier transformation (i.e., broader than 10 ps). In this case, the Fraunhofer approximation is not satisfied. In particular, we simulate the LCFG response to an ideal squared pulse with duration of 100 ps. The incident signal is identical to the one analyzed in Fig. 3(a), except for the obvious scale changes in the time and frequency axes. Fig. 4 shows the time representation (bottom plot), frequency representation (left plot), and joint time–frequency representation (Wigner–Ville distribution) of the resultant signal at the system's output. As in the last case, the output signal retains an energy density spectrum identical to that of the input signal. Again, the spectral components undergo a temporal realignment process following the linear dispersion characteristic of the
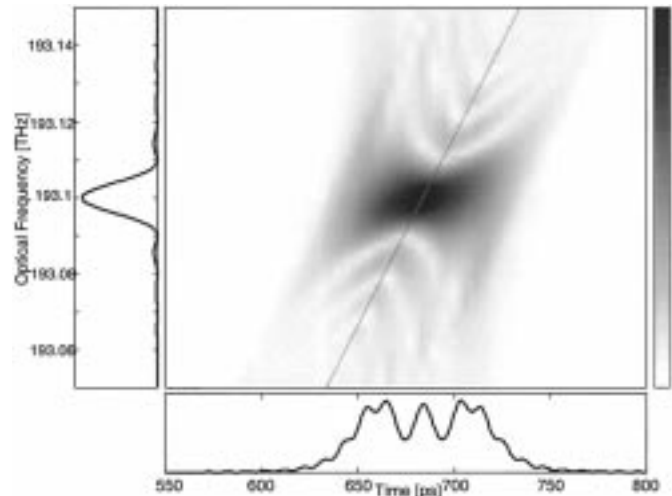

Fig. 4. Output signal from the real-time spectrum analyzer when the input signal is an ideal 100-ps-wide squared pulse (out of temporal Fraunhofer conditions), with the same definitions as for Fig. 3(a).
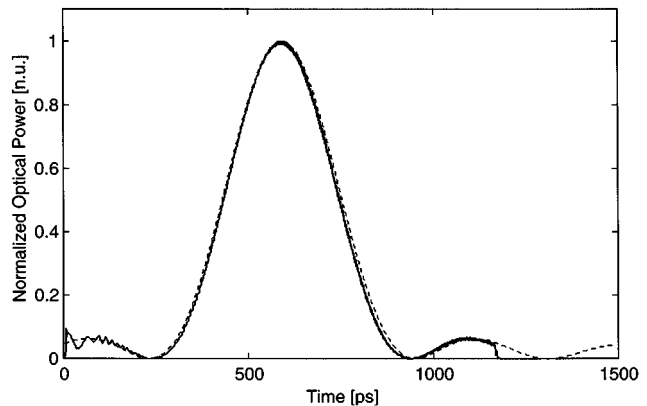

Fig. 5. Results from simulation of the real-time spectrum analyzer when the input signal is an ideal squared pulse 3 ps wide (out of bandwidth design conditions). Solid curve: normalized average power at the system's output. Dashed curve: energy density spectrum of the input signal envelope with $t_R(\text{ps}) = f(\text{THz}) \times 10^3$. [n.u.] stands for normalized units.

grating (depicted by the dashed line over the time–frequency plot). However, in this case, the temporal realignment is not sufficiently strong to get an effective temporal separation of the signal spectral components. It can be observed that the output signal energy is distributed in a wider frequency band at each moment of time. As a consequence, the time waveform of the reflected signal does not correspond to the spectrum of the input signal. In fact, this time waveform is easily identifiable with a Fresnel diffraction pattern for a square aperture [24].

To analyze the opposite case, we now consider an input pulse that verifies the requirements for Fourier transformation (Fraunhofer approximation) but whose bandwidth is broader than the grating's bandwidth. This case includes pulses narrower than those fixed for the design and also several broad-band pulses having time widths within the design interval. In these cases, the Fourier transformation is carried out but only over the grating bandwidth, which is a fraction of the input pulse's bandwidth. As an example, Fig. 5 shows the simulation results for an ideal
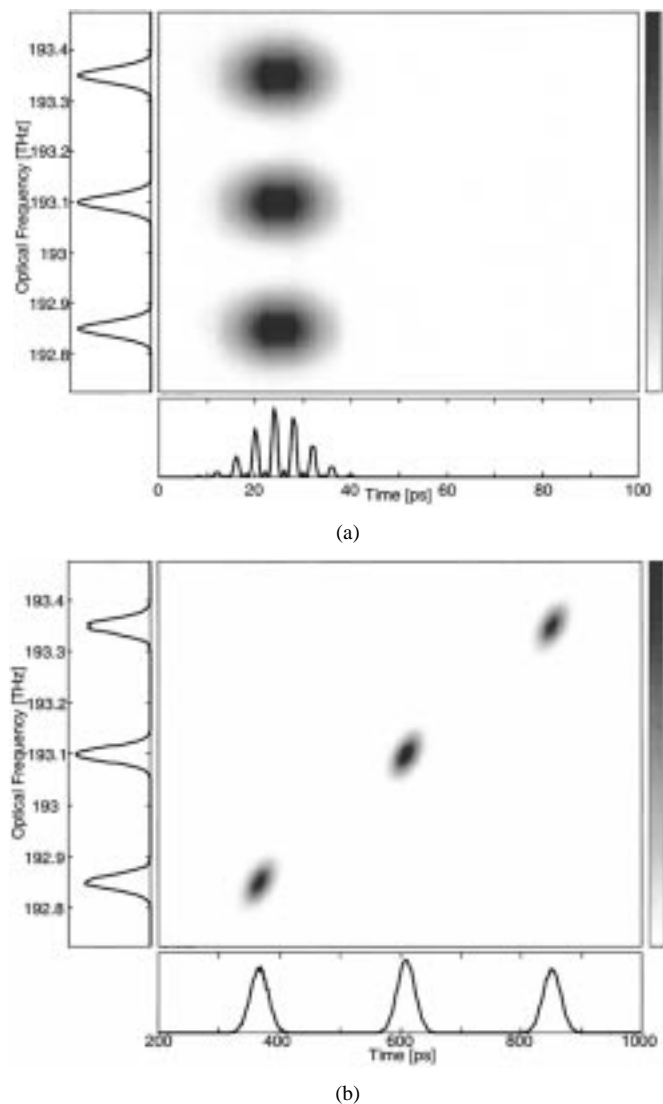
Fig. 6. Results from the simulation of the real-time spectrum analyzer, taking, as the input signal, a multi-frequency single pulse, which is composed of three 8-ps-rms-wide Gaussian pulses with identical time averages and modulated at different frequencies (detuned from the center frequency of 193.1 THz by −250, 0, and 250 GHz). (a) Input signal. The plot at the bottom shows the signal in the time domain. The plot on the left shows the signal in the frequency domain. The larger plot shows the joint time–frequency representation of the signal, by using the Spectrogram distribution. (b) Output signal, with the same definitions as for (a).

squared pulse with a duration of 3 ps. The figure shows the normalized optical power at the system's output (solid curve). The result is compared with the normalized energy density spectrum of the input signal envelope, which is represented in the same figure (dashed curve), changing the scale according to the (8), $t_R(\text{ps}) = f(\text{THz}) \times 10^3$. The bandwidth of the input pulse is broader than the grating's bandwidth (1.2 THz) and, therefore, only the spectrum over this bandwidth is recovered, i.e., the reflected signal extends over 1200 ps, which coincides with the grating's bandwidth of 1.2 THz, using the stated scale change.

We now analyze the system response to a multi-frequency single pulse. In particular, we consider a signal composed of three Gaussian functions with the same average time (25 ps) and rms time width (8 ps), but modulated at different frequencies (detuned from the center frequency of 193.1 THz by −250,

0, and 250 GHz). The time, frequency, and joint time–frequency representations of this signal are shown in Fig. 6(a). We now use the Spectrogram distribution [22], [23] for the time–frequency representation. The representation shows the three components of the input signal, which are separated in frequency but coincide in time. The signal obtained at the system's output is shown in Fig. 6(b). Since the input signal verifies the required conditions for the Fourier transformation, the time waveform of the output signal (bottom plot) coincides with the energy density spectrum of the input signal envelope. In this way, we can generate a train of temporal pulses from a multifrequency (multiwavelength) source. Furthermore, the joint time–frequency representation shows that these pulses are separated simultaneously in both time and frequency. In this particular case, the resultant pulses are separated by 250 ps, which correspond to the spectral separation of 250 GHz (with the scale change of $t_R(\text{ps}) = f(\text{THz}) \times 10^3$). It is worth noting that this type of signal (multiwavelength train of pulses) has been previously proposed for several applications in wavelength-division-multiplexed systems [28].

Finally, we study the system behavior with pulse sequences. In particular, we analyze the system response to a sequence of two Gaussian pulses. We assume 1-ps rms width pulses, separated by 8 ps. The average optical power corresponding to this signal, $P_1(t)$, is represented in Fig. 7(a). The optical power obtained at the system's output, $P_2(t)$], is shown in Fig. 7(b) (solid curve). This function practically coincides with the energy density spectrum $|\widehat{A}_1(\omega)|^2$ of the input signal envelope, which is represented in the same figure (dashed curve) by using the scale change in (8) ($t_R(\text{ps}) = f(\text{THz}) \times 10^3$). As in the corresponding spatial case (far-field diffraction from two slits), we obtain an interference pattern. The separation between peaks, as well as the width and intensity of these peaks, in the obtained pattern can be specifically tailored by varying the separation between pulses and the individual pulse characteristics (time width and intensity) of the input signal. This fact can be used for pulse-shaping applications. Here we center our attention on the relation between the separation between peaks in the output intensity pattern and the separation between the two input pulses. Let Δt_1 be the time distance between the input pulses and $\widehat{G}(\omega)$ the spectrum of each individual pulse. The energy density spectrum of the input signal envelope can then be expressed as $|\widehat{A}_1(\omega)|^2 = 2|\widehat{G}(\omega)|^2[1 + \cos(\Delta t_1 \omega)]$. By using the relation (7), the output average optical power can be written as

$$
\begin{aligned}
P_2(t) &= |\widehat{a}_2(t)|^2 \\
&= \frac{H_0^2}{\pi|\ddot{\Phi}_0|} \left\{ |\widehat{G}(\omega)|^2 [1 + \cos(\Delta t_1 \omega)] \right\}_{\omega = ((t - \dot{\Phi}_0)/\ddot{\Phi}_0)} \\
&= \frac{H_0^2}{\pi|\ddot{\Phi}_0|} \left| \widehat{G}\left(\omega = \frac{t - \dot{\Phi}_0}{\ddot{\Phi}_0} \right) \right|^2 \\
&\quad \cdot \left[1 + \cos\left(\frac{\Delta t_1}{\ddot{\Phi}_0} (t - \dot{\Phi}_0) \right) \right].
\end{aligned} \tag{12}
$$

The oscillatory nature of the output signal is due to the cosine function in the last equation. The period of this function is precisely the time separation between the peaks in the output op-
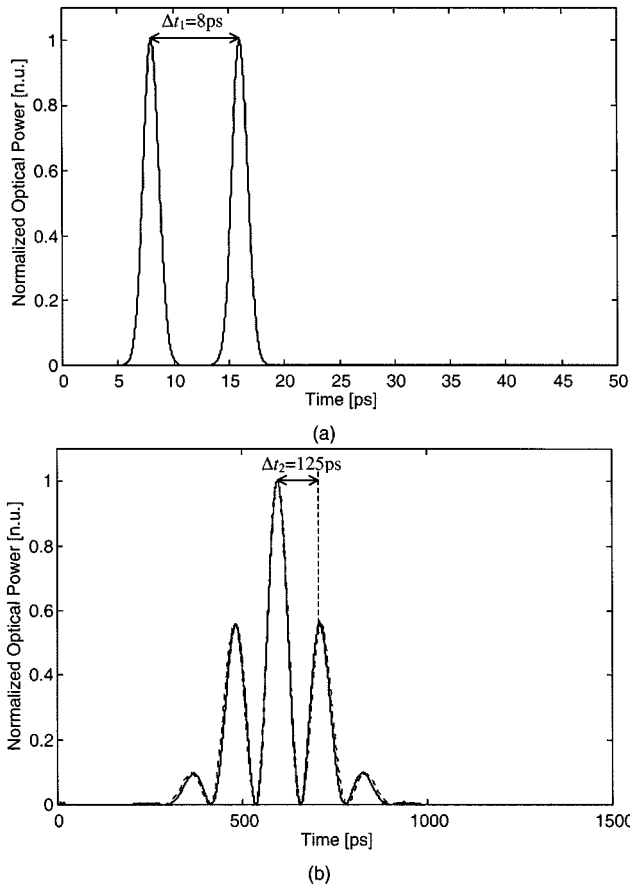
Fig. 7. Results from the simulation of the real-time spectrum analyzer. (a) Normalized average power of the input signal, which is composed of two Gaussian pulses of 1 ps-rms-width, separated by 8 ps. (b) Solid curve: normalized average power of output signal. Dashed curve: energy density spectrum of the input signal envelope with $t_R(\mathrm{ps}) = f(\mathrm{THz}) \times 10^3$. [n.u.] stands for normalized units.
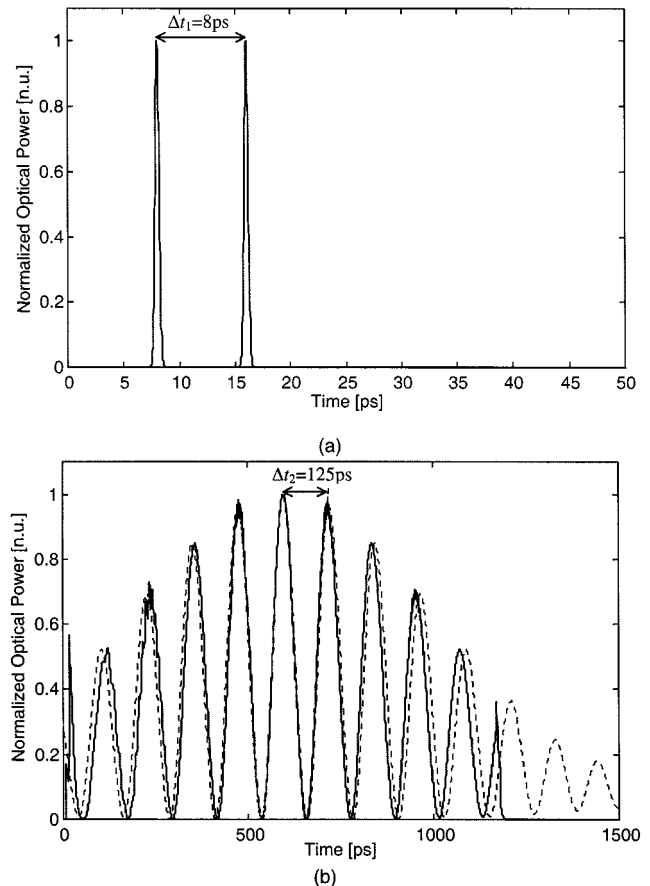

Fig. 8. Results from the simulation of the real-time spectrum analyzer out of bandwidth design conditions. (a) Normalized average power of the input signal, which is composed of two Gaussian pulses of 250 fs-rms-width, separated by 8 ps. (b) Solid curve: normalized average power of output signal. Dashed curve: energy density spectrum of the input signal envelope with $t_R(\mathrm{ps}) = f(\mathrm{THz}) \times 10^3$. [n.u.] stands for normalized units.

tical power Δt_2. Therefore, this time separation depends on the time distance between the input pulses Δt_1 according to the relation

$$\Delta t_2 = \frac{2\pi|\ddot{\Phi}_0|}{\Delta t_1}. \tag{13}$$

For instance, in the considered case, since $\Delta t_1 = 8$ ps and the grating dispersion $2\pi\ddot{\Phi}_0 = 10^3$ ps^2, we obtain a time separation between peaks in the output intensity pattern $\Delta t_2 = 125$ ps (see Fig. 7). In addition to its utility for tailoring the output signal characteristics, relation (13) provides a useful and easy means for measuring the first-order dispersion coefficient in chirped fiber gratings (LCFG or LCIC). By reflecting two pulses separated by a short enough time duration (Δt_1) from the grating being characterized, we obtain an interference intensity pattern from which we can measure the temporal separation in the intensity peaks (Δt_2). The grating dispersion coefficient $\ddot{\Phi}_0$ can then be determined using (13). The stated relations are also valid for pulses with a bandwidth broader than the designed bandwidth. As an example, we consider 250 fs rms-width Gaussian pulses, separated by 8 ps [Fig. 8(a)]. The time duration of the sequence is within the design interval (1–10 ps). However, the bandwidth of the individual pulse is broader than the LCFG bandwidth. As a result, the real-time Fourier transformation is carried out

but only over a fraction of the input signal's bandwidth (the grating's bandwidth). Fig. 8(b) shows the normalized optical power at the system's output (solid line) and the normalized energy density spectrum of the input signal envelope (dashed line). The output signal has a total duration of 1200 ps, which corresponds to the grating bandwidth of 1.2 THz. As predicted by theory, the temporal separation between the intensity peaks is again fixed to 125 ps.

V. CONCLUSIONS

We have used the temporal analog of spatial Fraunhofer diffraction to design real-time optical spectrum analyzers, using as dispersive media filtering devices based on chirped distributed resonant coupling. We present a unified approach for the design of LCFG's (reflection configurations) or LCIC's (transmission configurations) to carry out the proposed optical spectrum analysis. We have tested our designs by means of simulation tools for the cases of single pulses and pulse sequences. The results obtained from simulation show a very good agreement with those predicted by the theory. Furthermore, we have used the joint time–frequency signal analysis to get a deep insight into the physical effects that determine the performance of the proposed systems. In this

way, we have demonstrated that the propagation of a signal through an LCFG or LCIC, specifically designed to verify the temporal Fraunhofer conditions, translates into a temporal separation of the spectral components of this signal. This effect provides key abilities to modify and control the characteristics of temporal signals and, in consequence, can find important applications in the fields of temporal signal processing, optical communications, and other scientific areas.

Single-mode optical fiber or any of the resonant configurations proposed for dispersion compensation could be used as alternatives to the LCFG (LCIC) in order to yield the real-time spectrum analysis. The design of an optical fiber which verifies the required dispersion conditions leads, in general, to too long a distance for practical implementation, whereas the requirements of dispersion and bandwidth are usually contradictory in resonant system (the higher the dispersion, the narrower the bandwidth). However, in the LCFG (LCIC) design, these two requirements can be chosen independently. This fact makes these devices optimal candidates for carrying out the proposed as well as for implementing other interesting time-domain equivalents of well-known spatial systems [14], [15]. In general, the practical implementation of such systems opens important new perspectives in the mentioned fields.

ACKNOWLEDGMENT

REFERENCES

[1] E. B. Treacy, "Optical pulse compression with diffraction gratings," *IEEE J. Quantum Electron.*, vol. QE-5, pp. 454–458, Sept. 1969.

[2] A. Papoulis, "Pulse compression, fiber communications, and diffraction: A unified approach," *J. Opt. Soc. Amer. A*, vol. 11, no. 1, pp. 3–13, January 1994.

[3] B. H. Kolner, "Space-time duality and the theory of temporal imaging," *IEEE J. Quantum Electron.*, vol. 30, pp. 1951–1963, Aug. 1994.

[4] T. Jannson and J. Jannson, "Temporal self-imaging effect in single-mode fibers," *J. Opt. Soc. Amer.*, vol. 71, no. 11, pp. 1373–1376, November 1981.

[5] B. E. A. Saleh and M. I. Irshid, "Collet-Wolf equivalence theorem and propagation of a pulse in a single-mode optical fiber," *Opt. Lett.*, vol. 7, no. 7, pp. 342–343, 1982.

[6] T. Jannson, "Real-time Fourier transformation in dispersive optical fibers," *Opt. Lett.*, vol. 8, no. 4, pp. 232–234, 1983.

[7] B. H. Kolner and M. Nazarathy, "Temporal imaging with a time lens," *Opt. Lett.*, vol. 14, no. 12, pp. 630–632, 1989.

[8] ——, "Temporal imaging with a time lens: Erratum," *Opt. Lett.*, vol. 15, no. 11, p. 655, 1990.

[9] M. T. Kauffman, A. A. Godil, B. A. Auld, W. C. Banyai, and D. M. Bloom, "Applications of time lens optical systems," *Electron Lett.*, vol. 29, no. 3, pp. 268–269, 1993.

[10] C. V. Bennet, R. P. Scott, and B. H. Kolner, "Temporal magnification and reversal of 100 Gb/s optical data with an up-conversion time microscope," *Appl. Phys. Lett.*, vol. 65, no. 20, pp. 2513–2515, 1994.

[11] A. W. Lohmann and D. Mendlovic, "Temporal filtering with time lenses," *Appl. Opt.*, vol. 31, no. 29, pp. 6212–6219, 1992.

[12] M. A. Muriel, J. Azaña, and A. Carballar, "Real-time Fourier transformer based on fiber gratings," *Opt. Lett.*, vol. 24, no. 1, pp. 1–3, 1999.

[13] J. Azaña, L. R. Chen, M. A. Muriel, and P. W. E. Smith, "Experimental demonstration of real-time Fourier transformation using linearly chirped fiber Bragg gratings," *Electron Lett.*, vol. 35, no. 25, pp. 2223–2224, 1999.

[14] J. Azaña and M. A. Muriel, "Technique for multiplying the repetition rates of periodic trains of pulses by means of a temporal self-imaging effect in chirped fiber gratings," *Opt. Lett.*, vol. 24, no. 23, pp. 1672–1674, 1999.

[15] ——, "Temporal talbot effect in fiber gratings and its applications," *Appl. Opt.*, vol. 38, no. 32, pp. 6700–6704, 1999.

[16] J. Kuhl and J. Heppner, "Compression of femtosecond optical pulses with dielectric multilayer interferometers," *IEEE J. Quantum Electron.*, vol. QE-22, pp. 182–185, Jan. 1986.

[17] O. E. Martínez, "3000 times grating compressor with positive group velocity dispersion: Application to fiber compensation in 1.3-1.6 μm region," *IEEE J. Quantum Electron.*, vol. QE-23, pp. 59–64, Jan. 1987.

[18] F. Oullette, J.-F. Cliche, and S. Gagnon, "All-fiber devices for chromatic dispersion compensation based on chirped distributed resonant coupling," *J. Lightwave Technol.*, vol. 12, pp. 1728–1738, Oct. 1994.

[19] F. Ouellette, "Dispersion cancellation using linearly chirped Bragg grating filters in optical waveguides," *Opt. Lett.*, vol. 12, no. 10, pp. 847–849, 1987.

[20] ——, "All-fiber filter for efficient dispersion compensation," *Opt. Lett.*, vol. 16, no. 5, pp. 303–305, 1991.

[21] N. M. Litchinitser, B. J. Eggleton, and D. B. Patterson, "Fiber Bragg gratings for dispersion compensation in transmission: Theoretical model and design criteria for nearly ideal pulse recompression," *J. Lightwave Technol.*, vol. 15, pp. 1303–1313, Aug. 1997.

[22] S. Qian and D. Chen, *Joint Time-Frequency Analysis: Methods and Applications*. Englewood Cliffs, NJ: Prentice-Hall, 1996.

[23] L. Cohen, *Time-Frequency Analysis*. Englewood Cliffs, NJ: Prentice-Hall, 1995.

[24] J. W. Goodman, *Introduction to Fourier Optics*, 2nd ed, New York: McGraw-Hill, 1996.

[25] M. A. Muriel, A. Carballar, and J. Azaña, "Field distributions inside fiber gratings," *IEEE J. Quantum Electron.*, vol. 35, pp. 548–558, Apr. 1999.

[26] K. Ennser, M. N. Zervas, and R. Laming, "Optimization of apodized linearly chirped fiber gratings for optical communications," *IEEE J. Quantum Electron.*, vol. 34, pp. 770–778, May 1998.

[27] K. Ennser, R. I. Laming, M. N. Zervas, M. Ibsen, and M. Durkin, "Effects of nonideal group delay and reflection characteristics of fiber grating dispersion compensators," in *Proc. Eur. Conf. Optical Communications, 1997 (ECOC'97)*, vol. 2, pp. 45–48.

[28] L. R. Chen, S. D. Benjamin, P. W. E. Smith, and J. E. Sipe, "Applications of ultrashort pulse propagation in Bragg gratings for wavelength-division multiplexing and code-division multiple access," *IEEE J. Quantum Electron.*, vol. 34, pp. 2117–2129, Nov. 1998.

José Azaña (S'99) was born in Toledo, Spain, on December 8, 1972. He received the Ingeniero de Telecomunicación degree (M.S.) from the Universidad Politécnica de Madrid in 1997. He is currently working toward the Ph.D. degree at the Departamento de Tecnología Fotónica in the Universidad Politécnica de Madrid, where he is working on time–frequency representations and temporal signal processing in the field of photonics

His interests also include light propagation in periodic structures, space–time duality, and ultrafast optical processes.

Miguel A. Muriel (M'84–SM'98) was born in Burgos, Spain, on October 19, 1955. He received the Ingeniero de Telecomunicación degree (M.S.) in 1978 and the Doctor Ingeniero de Telecomunicación degree (Ph.D.) *(summa cum laude)* in 1980, both from the E.T.S. Ingenieros de Telecomunicación of the Universidad Politécnica de Madrid.

Since 1979, he has been with E.T.S. Ingenieros de Telecomunicación, as Assistant Professor in 1980, an Associate Professor in 1983, and a Full Professor in 1989. He has published more than 120 international papers and conference contributions, in the fields of liquid crystals, optical bistability, optical chaos, pulse propagation in fibers, optical signal processing, integrated optics, fiber-optic structures for signal processing, linear, and nonlinear resonators, fiber-optics sensors, fiber Bragg gratings, and time-frequency analysis. He has led ten research engineering projects, some of them with Spanish and European industries, and he has also acted as Technical Reviewer for several journals in the field of optoelectronics and optical communications. He has taught courses on optical electronics, optical communications, Fourier optics, electrooptical devices, and lasers. His professional interests cover fiber gratings, time–frequency representations, space–time duality, and, in general, signal processing applied to photonics and optical communications. He was Head of the Departamento of Tecnología Fotónica at the Universidad Politécnica de Madrid from September 1989 to October 1997.

Prof. Muriel is a member of the Optical Society of America. He received three awards for the Best Doctoral Thesis from the Universidad Menendez y Pelayo, Universidad Politécnica de Madrid, and Colegio de Ingenieros de Telecomunicación. He has received the Junior Research Award of the Universidad Politécnica de Madrid in 1989 and the Senior Research Award of the Universidad Politécnica de Madrid in 1998.